ORCID: 0000-0002-0555-7516

O. Yu. Liashenko
PhD, Univ. Grenoble Alpes, CNRS, Grenoble INP, SIMAP,
38000 Grenoble, France,
dr.oleksii.liashenko@gmail.com

D. Bouvard
Professor, Univ. Grenoble Alpes, CNRS, Grenoble INP, SIMAP,
38000 Grenoble, France,
didier.bouvard@grenoble-inp.fr

R. Dendievel
Professor, Univ. Grenoble Alpes, CNRS, Grenoble INP, SIMAP,
38000 Grenoble, France,
remy.dendievel@phelma.grenoble-inp.fr

УДК 62-405.6:62-405.8 PACS 62.20.−x, 61.43.Gt, 61.66.Dk, 61.66.Fn, 61.72.−y, 68.65.−k

DOI: 10.31651/2076-5851-2020-16-25

PROCESSING OF HYBRID STRUCTURES BY PARTIAL SINTERING OF TI-6AL-4V POWDER INTO EBM LATTICES[1]

A new approach of coupling additive manufacturing and conventional sintering methods for the fabrication of dense-porous hybrid structures with complex geometries and controlled porosity is presented. The critical effects of the procedure used to fill host electron-beam printed dense structures are investigated. The occurrence of flaws in the powder packing and their changes after different sintering cycles are emphasized. It is concluded that manual filling of the printed boxes after their complete de-powdering provides defect-poor structure with good interfaces between the dense and porous zones.

Keywords: Additive manufacturing, controlled sintering, hybrid structures, titanium alloys, microstructure.

1. Introduction

Fabrication of porous structures such as filters, bone implants or heat exchangers with adequate mechanical properties and controlled porosity is a challenging domain extensively studied during the last decade [1-3]. The final parts may need a complex architecture, with the coexistence of porous and dense zones, the latest ensuring the mechanical strength. Due to the hybrid nature of the final part, it is relevant to use a fabrication process mixing the recently developed additive manufacturing techniques and the more classical methods such as controlled sintering.

Controlled sintering and space holding techniques are used for the fabrication of homogenous porous structures [4-10] or structures with sharp gradients of porosity [11,12]. An important advantage of these methods is their applicability for production of large parts, but the mechanical strength of materials with high porosity can be rather low [8].

Metal additive manufacturing techniques, in which metal parts are printed by selectively melting a powder bed with a focused beam following a sliced CAD model, have extensively been developed during the last decade. The most common are Laser Beam Melting (LBM) and Electron Beam Melting (EBM) techniques [13]. In number of studies [3,14-21], lattices with different

[1] This work has been funded by ANR within ANR-14-ASTRID-0017 project. The authors are also thankful to Labex CEMAM for its contribution to the funding of the EBM equipment.

geometries were fabricated and the effect of cell geometry and global porosity of printed structures on their mechanical strength and fatigue resistance was investigated. EBM gives several advantages while printing Ti-based alloys, as lower oxidation of final part surface and elimination of internal residual stresses due to the vacuum level and the elevated temperatures during process, respectively [22,23]. However, these techniques are limited by the size of the smallest controllable geometric element (e.g., dense strut or pore), which is about 0.2 mm for LBM and 0.5 mm for EBM. A solution that has been proposed for fabricating materials with smaller pores involves partial melting of the powder by varying the beam intensity or the scanning speed [16,24], but the lack of process control leading to non-homogeneously distributed porosity is reported.

Hence, the conventional sintering and additive manufacturing methods have important limitations and cannot meet alone all the requirements for the fabrication of the aforementioned hybrid structures. An interesting approach is to couple both techniques in order to overcome element size restriction of additive manufacturing and mechanical strength issues of conventional sintering techniques. In this case the lattice structure serves both as a load bearing architecture and as a hosting structure for the porous part. Normally EBM process includes complete de-powdering stage but recently Ikeo and Nakano [25,26] printed closed boxes with internal vertical walls and preserved the inherited powder. The obtained hybrid structures were thermally treated in order to activate sintering of the residual powder around the dense printed structure**.** Such treatment was reported to increase the mechanical properties of the hybrid structure. Nevertheless, this approach may have some deficiencies if the printed structures have complex geometries. Also, in this case, the sintered powder is necessarily the powder of the AM process.

An alternative proposed in the present paper consists in filling the de-powdered lattice with a given powder after the EBM process. It can be the same powder used for EBM or another powder of different size, shape or chemical composition in case of suitable reactivity with the basic lattice material. Ti-6Al-4V alloy has been chosen as it is frequently selected in various applications for its lightness, biocompatibility, high strength, toughness and corrosion resistance [1,27-31]. In the following we will compare two procedures for producing Ti-6Al-4V hybrid structures based on EBM-printed lattices filled with powder: the Ikeo and Nagano procedure preserving the powder inherited from EBM process and a novel one consisting in manual powder filling of the lattices. The resulting microstructures and structures will be characterized by optical microscopy, scanning electron microscopy and X-ray microtomography. The effect of the filling procedure and thermal treatment will be investigated.

2. Experimental

The hosting structure is an open cubic box of 12 mm side with 1 mm thickness walls containing an octet-truss unit cell [19,32] with strut diameter being around 2 ± 0.1 mm (Figure 1a). This structure has been produced by Electron Beam Melting with an Arcam AB® A1 machine. The EBM process has been widely described in the literature, see e.g. [13]. It occurs under vacuum, typically 2×10^{-3} mbar. An important feature is that each layer undergoes a preheating stage, maintaining the building temperature around 700°C. This preheating leads to a slight sintering of the powder, which prevents local accumulation of negative charges and holds in place the powder. The starting powder is a Ti-6Al-4V plasma atomized spherical powder provided by ARCAM. The particle size is in the range 45 - 110 μm, with a median size of 75 μm and a tapped relative density around 0.63. It is customary to re-use particles that are not been melted in the EBM process. This means that the powder considered in the following had underwent several preheating stages.

The first type of hybrid structure was obtained by de-powdering the non-melted particles all around printed boxes and preserving them inside the boxes (Figure 1b). Such structures with powder inherited from EBM process (and thus slightly sintered) are denoted as *in-process filled* (IP) structures. The second type of hybrid structure was obtained by completely de-powdering the cubic boxes and subsequently filling them manually with the same ARCAM Ti-6Al-4V powder used for the EBM fabrication. Thus this powder underwent the same thermal treatment prior to the filling operation as in the previous case. The filling procedure consisted in gradual adding of powder while

tapping it in order to achieve compact packing of spherical particles inside the printed boxes. Such structures are denoted as *after-process filled* (AP) structures.

We have thus two kinds of components with the same hosting structure, filled with the same powder. For the first ones (IP) the powder has been slightly sintered during the EBM process, whereas for the second ones (AP) the powder has been simply poured and tapped. These two structures will be called as "as-received" and respectively denoted IP AR and AP AR. A subsequent heat treatment was then performed in a metallic furnace under a controlled atmosphere. In order to limit the amount of oxygen, the chamber was purged with pure argon and pumped until a vacuum of 1×10^{-2} Pa was attained. Two different thermal cycles were applied in order to activate sintering: one at low temperature (LT) with holding at 900°C for one hour and the other at high temperature (HT) with holding at 1300°C for one hour (Figure 1c). In both cases, the temperature rate during heating and cooling was 10°C/min.

In order to get a reference material, re-used Ti-6Al-4V powder has been poured and tapped in a cylindrical zirconia crucible (AR state) and sintered following both sintering cycles.

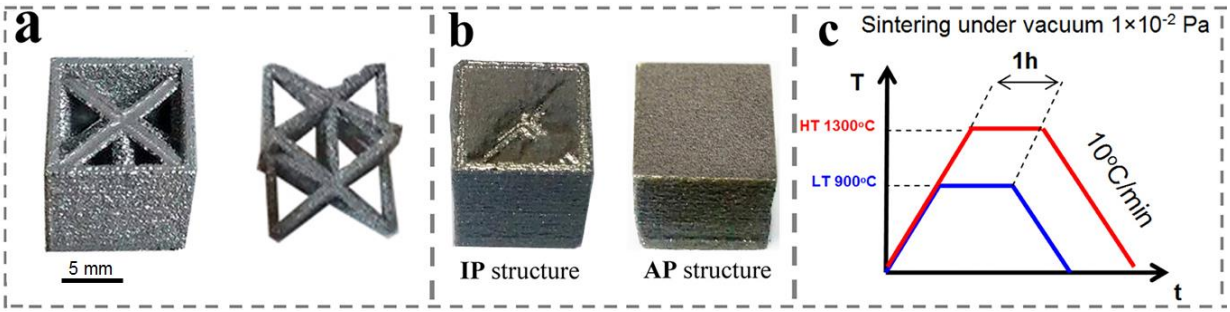

Fig. 1. Experimental route of producing hybrid structures: initial EBM-printed boxes with octet-truss lattice inside them (a), IP and AP filled structures (b) and thermal treatment profiles (c).

Рис. 1. Експериментальний метод виробництва гібридних структур: початкові EBM-друковані короби з октетною граткою всередині (a), структури заповнені під час друку (IP) та після друку (AP) (b) та профілі їх термічної обробки (c).

The powder densification in the boxes was observed by X-ray tomography using Phoenix V system. The voxel size was equal to 6 µm, allowing 3D reconstruction of elements larger than 12 µm with use of the ImageJ software and in-laboratory developed plugins. Such resolution is sufficient to detect the appearance of high porosity zones (referred to as flaws in the following) with a size at least equal to the average particle size. For particle packing and microstructure investigation the samples were cross-sectioned, prepared by conventional metallographic methods and observed by optical microscopy (OM) and SEM operating in backscatter mode.

The OM and SEM images were analyzed in order to calculate the fractions of observed phases, including the relative density, ρ_r, of the partially sintered powder in central flaw-free zones. The relative density is defined as the volume (or area, assuming the material is isotropic) of solid phase divided by the total volume (or area). To quantify the volume of previously reported flaws, the following dimensionless parameter, called relative flaw volume, is defined:

$$V_{fr} = (V_{pt} - V_{pn}) / V_{pt} \quad (1)$$

where V_{pt} is the total pore volume of the filled structure and V_{pn} is the volume of the porosity of the flaw-free zone including normally packed particles. V_{pt} has been measured by saturating the filled structure with ethanol and V_{pn} has been calculated by weighting the mass of the filling powder and measuring the average packing density from OM cross-section images.

3. Results and discussion

3.1. The reference material microstructure

In Figure 2 the reference material is observed by OM in the as-received state and after either sintering cycle. This re-used powder has a spherical morphology and a similar size distribution as the powder received from ARCAM (Figure 2a). It was kept inside the chamber at elevated temperature around 700°C for several hours, which was sufficient for the development of acicular α + β microstructure inside it with appearance of misoriented submicronic α needles (dark phase on micrograph built in Figure 2a) [33].

After the LT cycle the general microstructure consists of partially sintered spherical powder with interparticle necks having a diameter less than 10 μm (Figure 2b). The relative density, ρ_r, deduced from the micrograph is 0.644, which is a little higher that the nominal tapped density. After the LT cycle (Figure 2b) the internal microstructure exhibits misoriented α plates with a size in the range 2-5 μm decorated with the β phase. The fraction of the α phase is measured to be ~ 80%**.**

After the HT cycle (Figure 2b), interparticle necks have significantly grown, some of them reaching 50 μm diameter, and the relative density is ρ_r = 0.71. The internal microstructure is lamellar, with α lamellas having a width of 3-12 μm and the α-fraction being equal again to ~ 80%. It indicates that an α + β equilibrium is attained during cooling below the β transus temperature.

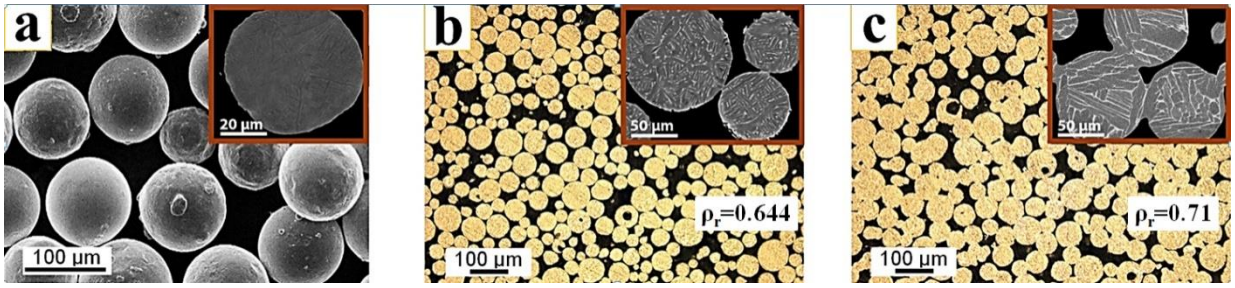

Fig. 2. Optical and SEM micrographs showing cross sections of representative microstructures of the reference material in the as-received state (a), after LT (b) and HT (c) cycles. In the built-in micrographs of the internal microstructure, the white zones are the β phase and the dark zones are the α - phase.

Рис. 2. Оптичні та SEM мікрофотографії, що демонструють перерізи представлених мікроструктур еталонного матеріалу в початковому стані (a), після циклів низько (LT) (b) та високотемпературної обробки HT (c). На мікрофотографіях внутрішньої мікроструктури, білі зони відповідають β-фазі, а темні — α-фазі.

3.2. The hybrid material microstructure

Figures 3a-c display virtual cross sections extracted from X-ray tomography images of the IP material in the AR state and after both sintering cycles. The relative density ρ_r is 0.56, 0.58 and 0.65 in the AR state, after 900°C sintering and after 1300°C sintering, respectively. It means that the particle packing in AR structure is much looser than the regular packing. Flaws are found below every inclined strut in AR state. As it can be seen from local 3D rendering (see the upper part of Figure 3) these flaws have a thickness around 130 μm for the sample in AR state and they are curved in accordance with the surface of the struts above them. Their average thickness has increased to 150 μm after LT treatment and to 350 μm after HT treatment. Meanwhile the relative flaw volume, V_{fr}, defined in Eq. 1 is 0.35, 0.37 and 0.51 in AR, LT and HT structures, respectively. These values point out on the large volume taken by flaws and the loss of homogeneity of the porous part of the hybrid structure.

The bottom parts of Figures 3a-c show details of the interface between the upper surfaces of the lower lattice struts and the porous parts of the hybrid structures. As it can be seen in Figure 3a, tiny necks with a few microns diameter can be found in these zones, which is due to the preheating at 700°C in the EBM machine chamber. After LT and HT sintering cycles these necks are growing in

diameter with size being similar to the interparticle necks developed during same thermal treatments of the reference material.

A very fine, basket-weaved, Widmänstatten-type microstructure is developed inside as-built lattices (see bottom part of Figure 3a). The observed α laths have an average width ~ 0.5 ± 0.2μm similar to the microstructure reported in previous studies [19,34]. As it can be seen from Figures 1b,c the α-plates observed inside the sintered powder of hybrid structures and inside the printed lattice struts are identical to the ones observed in the reference material. It means that the thermal treatments not only yield the mechanical consolidation of the dense and porous parts of the hybrid structures, but also lead to the certain homogeneity of the microstructures developed inside these materials.

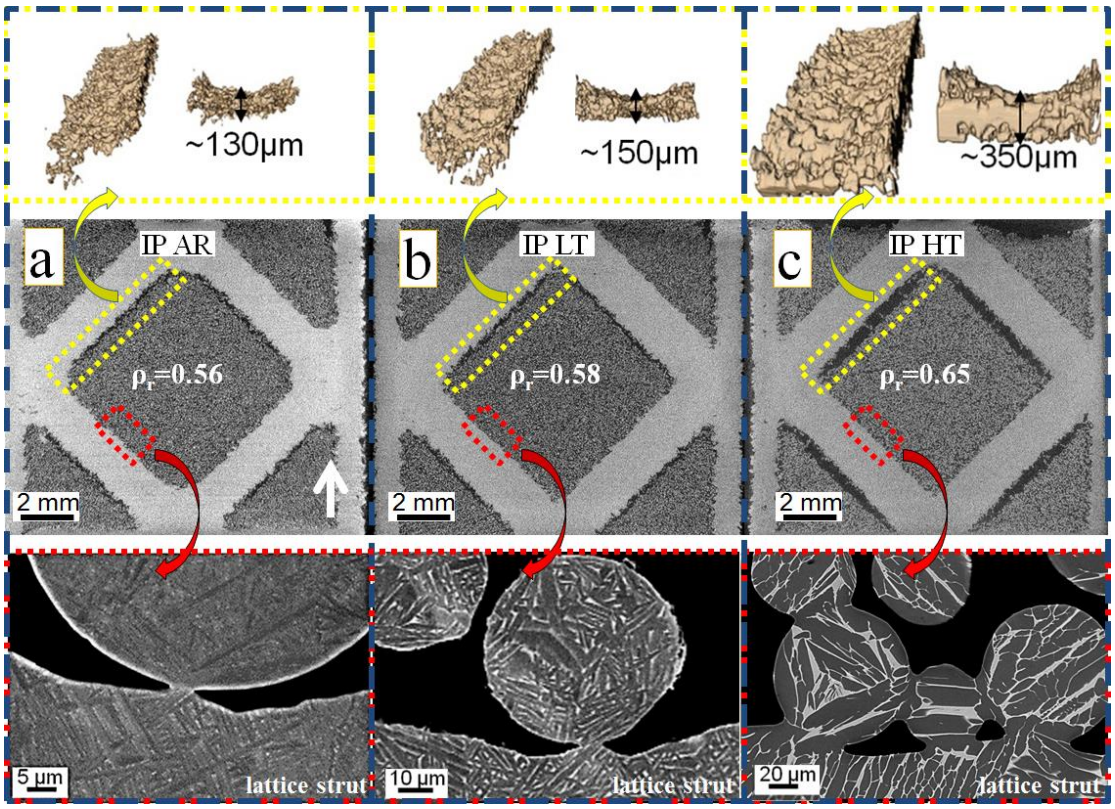

Fig. 3. Virtual cross sections of X-ray tomography images of IP produced structures and 3D rendering of flaws in AR state (a) and after LT (b) and HT (c) sintering cycles. White arrow indicates the build direction. The upper parts display the 3D rendering of flaws found below the inclined struts of lattice structures. The bottom parts show the microstructures inside the partially sintered particles and the printed lattice in the contact zones.

Рис. 3. Віртуальні поперечні перерізи на основі рентгенівської томографії структур заповнених в процесі друку (IP) і 3D-рендер дефектів в початковому стані (AR) (a) та після низько (LT) (b) та високотмпературного (HT) (c) циклу спікання. Біла стрілка вказує на напрям друку. На верхніх зображеннях приведено 3D-рендер дефектів поблизу похилих елементів внутрішніх граток. На нижніх зображеннях приведено мікроструктуру частково спечених порошинок і друкованої гратки в контактній зоні.

In Figure 4 virtual cross sections of tomography images of the AP structures are presented. The relative density, ρ_r, is 0.63, 0.64, 0.7 in the AR state, after 900°C sintering and after 1300°C sintering, respectively. These values are very close to the ones found for the reference material, which proves that the AP process results in a dense packing and that the sintering course is not affected by the presence of the struts. No significant flaw is observed in the AR structure nor in the LT sintered one. However, slight packing faults are detected just below the upper and bottom strut junctions (see the dashed arrows in Figure 4a,b), which can be due to the difficulty to fill manually all the hardly

accessible zones. These packing faults resulted in a value V_{fr} = 0.14 for LT structure, which is 2.5 and 2.65 times lower than the respective values obtained for as-received and LT sintered IP-filled structures. After the HT cycle, needle-like flaws with thickness linearly increasing up to 250 μm is found under the upper parts of the inclined struts and the total flaw volume has got more significant (V_{fr} = 0.36).

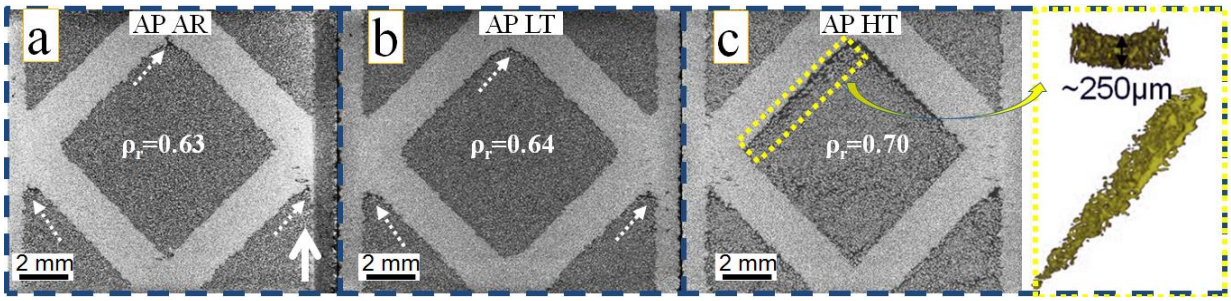

Fig. 4. Virtual cross sections of X-ray tomography images of AP-filled structures in AR state (a) and after LT (b) and HT (c) sintering cycles. The dashed arrows indicate the packing faults below upper and bottom strut junctions in as-received state and after LT sintering cycle. The 3D rendering of a flaw developed after HT sintering cycle is in the right built-in image.

Рис. 4. Віртуальні поперечні перерізи за даними рентгенівської томографії структур заповнених після друку (AP) в початковому стані (AR) (a) та після низько (LT) (b) та високотмпературного (HT) (c) циклу спікання. Біла стрілка вказує на напрям друку. Пунктирні лінії вказують на дефекти пакування в нижній і верхній зоні з'єднань елементів граток. На вбудованому зобрадені з правого боку показано 3D-рендер дефекту, який утворився після високотмператорного спікання.

A comparison of Figures 3 and 4 clearly indicates the benefit of the manual powder filling. This method allows reaching the theoretical packing density of powder inside the printed boxes, leading to the better control of the partial sintering of the powder at low temperatures (sintering at $T/T_{m\text{-}}$(solidus) ≈ 0.54 leads to a densification of 1.5% in 1 hour). Hence, the best result in terms of defects was obtained when applying the LT profile to the AP filled structures (see Figure 4b).

Nevertheless, attention should be paid to the completeness of the filling procedure as some zones might be hardly accessible to the powder particles. We believe that such difficulties may be resolved by applying long-time vibrations on the open boxes over-filled with a given powder.

4. Conclusions

A method for fabricating Titanium alloy based dense-porous hybrid structures by coupling EBM printing of boxes with internal lattices and partial sintering of powder filled inside has been presented. Two different filling procedures and two sintering temperatures have been compared. It has been found that the faster procedure that consists in keeping the powder inherited from the EBM process inside the boxes has serious limitations : loose particle packing and formation of large defects below the inclined lattice struts and their further growth during sintering. In its turn, manual filling of the printed boxes after their complete de-powdering resulted in dense and defect-poor packing with good interfaces between the dense and porous parts of the hybrid structure. Formation of the lamellar structures with similar colonies of α-phase in the contact zones between porous and dense parts of hybrid structure has been displayed. The results of this study can be applied to fabricate mechanically reliable filters or heat exchangers as well as novel hybrid multimaterials with complex geometries.

References (in language original):

1. Lefebvre L. P., Banhart J., Dunand D. C. Porous metals and metallic foams: current status and recent developments //Advanced engineering materials. – 2008. – Т. 10. – №. 9. – С. 775-787.

2. Sidambe A. T. Biocompatibility of advanced manufactured titanium implants—A review //Materials. – 2014. – Т. 7. – №. 12. – С. 8168-8188.

3. Wang X. et al. Topological design and additive manufacturing of porous metals for bone scaffolds and orthopaedic implants: A review //Biomaterials. – 2016. – Т. 83. – С. 127-141.

4. Oh I. H. et al. Mechanical properties of porous titanium compacts prepared by powder sintering //Scripta Materialia. – 2003. – Т. 49. – №. 12. – С. 1197-1202.

5. Dunand D. C. Processing of titanium foams //Advanced engineering materials. – 2004. – Т. 6. – №. 6. – С. 369-376.

6. Chino Y., Dunand D. C. Directionally freeze-cast titanium foam with aligned, elongated pores //Acta Materialia. – 2008. – Т. 56. – №. 1. – С. 105-113.

7. Dewidar M. M., Lim J. K. Properties of solid core and porous surface Ti–6Al–4V implants manufactured by powder metallurgy //Journal of Alloys and Compounds. – 2008. – Т. 454. – №. 1-2. – С. 442-446.

8. Jorgensen D.J., D.C. Dunand. Ti–6Al–4V with micro-and macropores produced by powder sintering and electrochemical dissolution of steel wires //Mater. Sci. and Eng. A. – 2010. – Т. 527. – С. 849-853.

9. Pereloma E.V., Savvakin D.G., Carman A., Gazder A.A., Ivasishin O.M. Microstructure development and alloying elements diffusion during sintering of near-β titanium alloys // Key Eng. Mater. – 2012. – T.520. – C. 49-56.

10. Torres Y. et al. Development of porous titanium for biomedical applications: A comparison between loose sintering and space-holder techniques //Materials Science and Engineering: C. – 2014. – Т. 37. – С. 148-155.

11. Lee J. H. et al. Characterization and deformation behavior of Ti hybrid compacts with solid-to-porous gradient structure //Materials & Design. – 2014. – Т. 60. – С. 66-71.

12. Ahmadi S., Sadrnezhaad S. K. A novel method for production of foamy core compact shell Ti6Al4V bone-like composite //Journal of Alloys and Compounds. – 2016. – Т. 656. – С. 416-422.

13. Murr L. E. et al. Metal fabrication by additive manufacturing using laser and electron beam melting technologies //Journal of Materials Science & Technology. – 2012. – Т. 28. – №. 1. – С. 1-14.

14. Krishna B. V., Bose S., Bandyopadhyay A. Low stiffness porous Ti structures for load-bearing implants //Acta biomaterialia. – 2007. – Т. 3. – №. 6. – С. 997-1006.

15. Yavari S. A. et al. Relationship between unit cell type and porosity and the fatigue behavior of selective laser melted meta-biomaterials //Journal of the mechanical behavior of biomedical materials. – 2015. – Т. 43. – С. 91-100.

16. Furumoto T. et al. Permeability and strength of a porous metal structure fabricated by additive manufacturing //Journal of Materials Processing Technology. – 2015. – Т. 219. – С. 10-16.

17. Heinl P., Mueller L., Koerner C., Singer R.F., Mueller F.A. Cellular Ti–6Al–4V structures with interconnected macro porosity for bone implants fabricated by selective electron beam melting //Acta Biomater. – 2008. – № 4. – С. 1536–1544.

18. Li S. J. et al. Influence of cell shape on mechanical properties of Ti–6Al–4V meshes fabricated by electron beam melting method //Acta biomaterialia. – 2014. – Т. 10. – №. 10. – С. 4537-4547.

19. Suard M. et al. Mechanical equivalent diameter of single struts for the stiffness prediction of lattice structures produced by Electron Beam Melting //Additive Manufacturing. – 2015. – Т. 8. – С. 124-131.

20. Cheng X.Y. et al. // J.Mech. Behav. Biomed. Mater . – 2012. – № 16. – С. 153–162.

21. Hernández-Nava E. et al. The effect of density and feature size on mechanical properties of isostructural metallic foams produced by additive manufacturing //Acta Materialia. – 2015. – Т. 85. – С. 387-395.

22. Tan X. et al. Graded microstructure and mechanical properties of additive manufactured Ti–6Al–4V via electron beam melting //Acta Materialia. – 2015. – Т. 97. – С. 1-16.

23. Galarraga H. et al. Effects of heat treatments on microstructure and properties of Ti-6Al-4V ELI alloy fabricated by electron beam melting (EBM) //Materials Science and Engineering: A. – 2017. – Т. 685. – С. 417-428.

24. Gaytan S. M. et al. Advanced metal powder based manufacturing of complex components by electron beam melting //Materials technology. – 2009. – Т. 24. – №. 3. – С. 180-190.

25. Ikeo N., Ishimoto T., Nakano T. Novel powder/solid composites possessing low Young's modulus and tunable energy absorption capacity, fabricated by electron beam melting, for biomedical applications //Journal of Alloys and Compounds. – 2015. – Т. 639. – С. 336-340.

26. Nakano T. et al //Proceedings of the 13th World Conference on Titanium, John Wiley & Sons. – 2016. – New Jersey. – С. 1679-1683.

27. Niinomi M. Recent metallic materials for biomedical applications //Metall. Mater. Tran. A. – 2002. – № 33. – 477.

28. Shah R. K., Sekulic D. P. Fundamentals of heat exchanger design. – John Wiley & Sons, 2003.

29. Ryan G., Pandit A., Apatsidis D. P. Fabrication methods of porous metals for use in orthopaedic applications //Biomaterials. – 2006. – Т. 27. – №. 13. – С. 2651-2670.

30. Singh R. et al. Titanium foams for biomedical applications: a review //Materials Technology. – 2010. – Т. 25. – №. 3-4. – С. 127-136.

31. Salvo L. et al. Processing and structures of solids foams //Comptes Rendus Physique. – 2014. – Т. 15. – №. 8-9. – С. 662-673.

32. Deshpande V. S., Fleck N. A., Ashby M. F. Effective properties of the octet-truss lattice material //Journal of the Mechanics and Physics of Solids. – 2001. – Т. 49. – №. 8. – С. 1747-1769.

33. Sun Y., Aindow M., Hebert R. J. The effect of recycling on the oxygen distribution in Ti-6Al-4V powder for additive manufacturing //Materials at High Temperatures. – 2018. – Т. 35. – №. 1-3. – С. 217-224.

34. Martin G. et al. Coupling electron beam melting and spark plasma sintering: A new processing route for achieving titanium architectured microstructures //Scripta Materialia. – 2016. – Т. 122. – С. 5-9.

References:

1. Lefebvre L. P., Banhart J., Dunand D. C. (2008). Porous metals and metallic foams: current status and recent developments. *Advanced engineering materials*, 10(9), 775-787.

2. Sidambe A. T. (2014). Biocompatibility of advanced manufactured titanium implants—A review. *Materials*, 2014, 7(12), 8168-8188.

3. Wang X. et al. (2016). Topological design and additive manufacturing of porous metals for bone scaffolds and orthopaedic implants: A review. *Biomaterials*, 83, 127-141.

4. Oh I. H. et al. (2003). Mechanical properties of porous titanium compacts prepared by powder sintering. *Scripta Materialia*, 49(12), 1197-1202.

5. Dunand D. C. (2004). Processing of titanium foams. *Advanced engineering materials*, 6(6), 369-376.

6. Chino Y., Dunand D. C. (2008). Directionally freeze-cast titanium foam with aligned, elongated pores. *Acta Materialia*, 56(1), 105-113.

7. Dewidar M. M., Lim J. K. (2008). Properties of solid core and porous surface Ti–6Al–4V implants manufactured by powder metallurgy. *Journal of Alloys and Compounds*, 454(1-2), 442-446.

8. Jorgensen D. J., Dunand D. C. (2010). Ti–6Al–4V with micro-and macropores produced by powder sintering and electrochemical dissolution of steel wires. *Mater. Sci. and Eng. A*, (527), 849-853.

9. Pereloma E. V., Savvakin D. G., Carman A., Gazder A. A., Ivasishin O. M. (2012). Microstructure development and alloying elements diffusion during sintering of near-β titanium alloys. *Key Eng. Mater.*, 520, 49-56.

10. Torres Y. et al. (2014). Development of porous titanium for biomedical applications: A comparison between loose sintering and space-holder techniques. *Materials Science and Engineering*, 37, 148-155.

11. Lee J. H. et al. (2014). Characterization and deformation behavior of Ti hybrid compacts with solid-to-porous gradient structure. *Materials & Design*, 60, 66-71.

12. Ahmadi S., Sadrnezhaad S. K. (2016). A novel method for production of foamy core compact shell Ti6Al4V bone-like composite. *Journal of Alloys and Compounds*, 656, 416-422.

13. Murr L. E. et al. (2012). Metal fabrication by additive manufacturing using laser and electron beam melting technologies. *Journal of Materials Science & Technology*, 28(1), 1-14.

14. Krishna B. V., Bose S., Bandyopadhyay A. (2007). Low stiffness porous Ti structures for load-bearing implants. *Acta biomaterialia*, 3(6), 997-1006.

15. Yavari S. A. et al. (2015). Relationship between unit cell type and porosity and the fatigue behavior of selective laser melted meta-biomaterials. *Journal of the mechanical behavior of biomedical materials*, 43, 91-100.

16. Furumoto T. et al. (2015). Permeability and strength of a porous metal structure fabricated by additive manufacturing. *Journal of Materials Processing Technology*, 219, 10-16.

17. Heinl P., Mueller L., Koerner C., Singer R.F., Mueller F.A. (2008). Cellular Ti–6Al–4V structures with interconnected macro porosity for bone implants fabricated by selective electron beam melting. *Acta Biomater*, 4, 1536–1544.

18. Li S. J. et al. (2014). Influence of cell shape on mechanical properties of Ti–6Al–4V meshes fabricated by electron beam melting method. *Acta biomaterialia*, 10(10), 4537-4547.

19. Suard M. et al. (2015). Mechanical equivalent diameter of single struts for the stiffness prediction of lattice structures produced by Electron Beam Melting. *Additive Manufacturing*, 8, 124-131.

20. Cheng X.Y. et al. (2012). *J.Mech. Behav. Biomed. Mater*, 16, 153–162.

21. Hernández-Nava E. et al. (2015). The effect of density and feature size on mechanical properties of isostructural metallic foams produced by additive manufacturing. *Acta Materialia*, 85, 387-395.

22. Tan X. et al. (2015) Graded microstructure and mechanical properties of additive manufactured Ti–6Al–4V via electron beam melting. *Acta Materialia*, 97, 1-16.

23. Galarraga H. et al. (2017). Effects of heat treatments on microstructure and properties of Ti-6Al-4V ELI alloy fabricated by electron beam melting (EBM). *Materials Science and Engineering: A.*, 685, 417-428.

24. Gaytan S. M. et al. (2009). Advanced metal powder based manufacturing of complex components by electron beam melting. *Materials technology*, 24 (3), 180-190.

25. Ikeo N., Ishimoto T., Nakano T. (2015). Novel powder/solid composites possessing low Young's modulus and tunable energy absorption capacity, fabricated by electron beam melting, for biomedical applications. *Journal of Alloys and Compounds*, 639, 336-340.

26. Nakano T. et al (2016). Proceedings of the 13th World Conference on Titanium, John Wiley & Sons, *New Jersey*, 1679-1683.

27. Niinomi M. (2002). Recent metallic materials for biomedical applications. *Metall. Mater. Tran. A.*, 33, 477.

28. Shah R. K., Sekulic D. P. (2003). Fundamentals of heat exchanger design. – *John Wiley & Sons*.

29. Ryan G., Pandit A., Apatsidis D. P. (2006). Fabrication methods of porous metals for use in orthopaedic applications. *Biomaterials*, 27(13), 2651-2670.

30. Singh R. et al. (2010). Titanium foams for biomedical applications: a review. *Materials Technology*, 25(3-4), 127-136.

31. Salvo L. et al. (2014). Processing and structures of solids foams. *Comptes Rendus Physique*, 15(8-9), 662-673.

32. Deshpande V. S., Fleck N. A., Ashby M. F. (2001). Effective properties of the octet-truss lattice material. *Journal of the Mechanics and Physics of Solids*, 49(8), 1747-1769.

33. Sun Y., Aindow M., Hebert R. J. (2018). The effect of recycling on the oxygen distribution in Ti-6Al-4V powder for additive manufacturing. *Materials at High Temperatures*, 35(1-3), 217-224.
34. Martin G. et al. (2016). Coupling electron beam melting and spark plasma sintering: A new processing route for achieving titanium architectured microstructures. *Scripta Materialia*, 122, 5-9.

О. Ю. Ляшенко
аспірант, Університет Гренобль Альпи, Національний центр наукових досліджень, Гренобльський технологічний інститут, SIMAP, 38000 Гренобль, Франція
dr.oleksii.liashenko@gmail.com

Д. Бувар
професор, Університет Гренобль Альпи, Національний центр наукових досліджень, Гренобльський технологічний інститут, SIMAP, 38000 Гренобль, Франція
didier.bouvard@grenoble-inp.fr

Р. Дендівель
професор, Університет Гренобль Альпи, Національний центр наукових досліджень, Гренобльський технологічний інститут, SIMAP, 38000 Гренобль, Франція
remy.dendievel@phelma.grenoble-inp.fr

ВИРОБНИЦТВО ГІБРИДНИХ СТРУКТУР ЗА ДОПОМОГОЮ ЧАСТКОВОГО СПІКАННЯ ПОРОШКІВ TI-6AL-4V У ЕЛЕКТРОННО НАПИЛЕНИХ ГРАТКАХ

Анотація. *Продемонстровано новий підхід поєднання технології пошарового друку металу з традиційними методами порошкової металургії для виготовлення щільних гібридних структур зі складною геометрією та контрольованою пористістю. Досліджено критичні ефекти процедури заповнення об'ємних структур надрукованих за допомогою плавлення порошку електронним пучком. Описані наявність дефектів в упаковці порошку та їх еволюція під час різних циклів спікання. Ручне заповнення друкованих коробів після повного видалення порошку забезпечує бездефектну структуру з бездефектним інтерфейсом між щільною та пористою частинами гібридної структури.*

Ключові слова: технологія пошарового друку металом, контрольоване спікання, гібридні структури, титанові сплави, мікроструктура.

Одержано редакцією 01.10.2020
Прийнято до друку 08.11.2020